8-8-2022

Origin of the electroarthrogram and streaming potentials in compressed cartilage

Charles F. Babbs

Hypothesis paper:

Origin of the electroarthrogram and streaming potentials in compressed cartilage

Charles F. Babbs, MD, PhD
Weldon School of Biomedical Engineering, Purdue University
August 8, 2022

Abstract

Background: The electroarthrogram (EAG) is a recording of electrical potentials near a joint, usually a knee, that are generated when the articular cartilage is rhythmically compressed by weight bearing. Physics-based, quantitative prediction of the magnitude of the electroarthrogram remains an open problem.

Methods and Results: A new electromechanical model is created to describe viscous displacement of sodium ions from fixed sulfonate anions in the cartilage matrix by radial flow of interstitial fluid during side-to-side shifting of body weight. The viscous force exerted by fluid flow slightly displaces the Na^+ ion in its potential energy well. The ion pairs form electrical dipoles, for which changes in measured electrical potential fields are calculated and integrated. The EAG signal from any small volume in a disk of cartilage is computable directly from a lumped physical constant, the radial distance from the center of the disk, the compressive strain rate, the local thickness of the cartilage, as well as other geometric and physical factors. There are no unknown free parameters. There are no arbitrary constants. The predicted amplitude of the EAG voltage for a normal human subject is 0.174 mV, compared to 0.035 mV for a person with moderate to severe osteoarthritis. These values are within the ranges of measured EAG amplitudes in humans.

Conclusions: The new model provides a first-principles, physically plausible explanation of streaming potentials in cartilage. The algebraic form of the equation predicting EAG amplitude offers insights into the key variables that determine the EAG signal and could lead to more informed and useful applications of electroarthrography.

Key words: biophysics, boundary layer, compression, cyclic loading, dipole, electrical potentials, electromechanical transduction, extracellular matrix, far field, fixed anions, fixed charge density, forward problem, glycosaminoglycans, knee, laminar flow, loading, matrix, osteoarthritis, proteoglycans, stiffness, strain, streaming potential, sulfonate, viscosity, zeta potential

INTRODUCTION

The electroarthrogram (EAG) is a curious electrical signal of sub-millivolt amplitude that is recorded by a skin surface electrode placed near the joint line of a weight-bearing knee joint. As weight is put on the knee during the loading phase, a positive voltage signal appears, shown in Figure 1, sketched from the experimental data of Preville and coworkers[1]. During unloading a corresponding negative signal is recorded. In a typical laboratory experiment, electrodes are placed over the medial and lateral aspects of the knee joint. The positive electrode on the joint line of the knee is paired with a negative or more distant reference electrode above or below the knee. The erect human subject slowly transfers full body weight side-to-side, from one standing leg to the other. The potential difference recorded between the electrodes constitutes the EAG signal. The waveform of the voltage signal in the time domain is roughly rectangular, as shown in Figure 1, with both positive and negative phases.

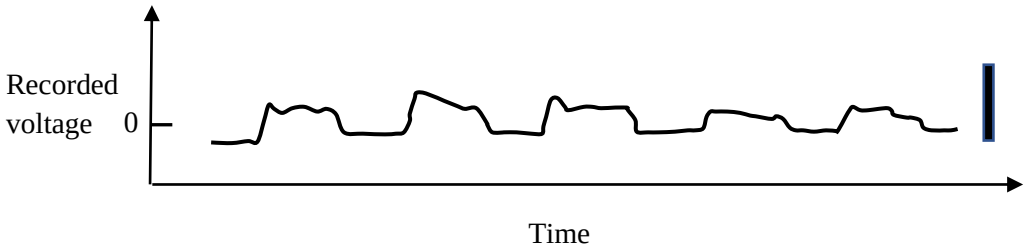

Figure 1. Sketch of an electroarthrogram from a normal human subject[1]. Rhythmic joint loading and cartilage compression are achieved by having the subject slowly shift weight from one leg to the other approximately every four seconds. The vertical bar represents 0.75 millivolts. The positive skin surface electrode was located at the joint line of the medial knee compartment. The negative reference electrode was placed over the shin, at a site with little skin movement, overlying bone. The peak-to-peak EAG displacement is ~ 0.25 mV. Here, as in electronics, "peak-to-peak" means the difference between the maximum positive voltage and the maximum negative voltage, adjusting for noise.

Acceptance of the EAG as a useful clinical tool and confidence in the interpretation of the data obtained would be greatly enhanced if people understood exactly how this unusual electrical signal is generated. The present paper explores the underlying biomechanics and physical chemistry of knee cartilage under cyclic compression to create a simple algebraic model that predicts the electrical potentials of the electroarthrogram.

Joint cartilage consists of a polymeric matrix made of collagen, proteoglycans, non-collagenous proteins, lipids, together with and embedded cells. The matrix is swollen with physiologic salt solution, essentially 1 percent sodium chloride in water. Negatively charged sulfonic acid ($-SO_3^-$) and carboxy acid ($-COO^-$) groups at physiologic pH are located predominantly on the chondroitin sulphate and keratan sulphate glycosaminoglycan (GAG) chains that are covalently

linked to the protein backbone of the matrix[2, 3], forming proteoglycans. The local concentration of these fixed negative charges is directly proportional to the glycosaminoglycan content[4]. When cartilage is compressed, a small amount of interstitial fluid, is squeezed from the matrix[5], which remains relatively fixed in space. The process is similar to slight compression of a wet sponge.

The cartilage compression causes a form of mechanical to electrical transduction, creating electric fields called streaming potentials, measured as the EAG. The streaming voltage is critically dependent on the density of fixed anions in the cartilaginous matrix. Fixed anions make cartilage slippery, enhancing its function. Increasing content of fixed anions also makes cartilage stiffer[6]. Both increased stiffness and thickness of the cartilage enhance load bearing and shock resistance[3, 4, 7]. Further, the fixed anion content, stiffness, and thickness are known to deteriorate with joint pathology in osteoarthritis[4, 8]. If the EAG signal were quantitatively related to these variables in a known way, then the EAG might well serve as a useful diagnostic test of joint health.

In words, the new mechanistic hypothesis of the present paper is as follows. As the knee cartilage is compressed between the femur and the tibia, a small amount of fluid is squeezed out **radially**. (This direction of fluid streaming is perpendicular to streaming studied by early investigators[5, 8, 9], in which electrical potentials were measured along the axis of compression, not perpendicular to it.) The cartilaginous matrix contains fixed negative charges attached to the polymeric matrix. These fixed anions are paired with electrostatically bound, positively charged sodium ions. Compression squeezes water radially from the center of the cartilage toward the periphery through pores in the cartilage matrix. The moving fluid slightly displaces mobile Na^+ ions relative to the solid phase containing the fixed R-SO_3^- ions. In particular, the layer of water molecules contacting a Na^+ ion creates a small local viscous drag, pushing the Na^+ ion in the direction of flow and simultaneously stretching its radial desistance from the companion -SO_3^- ion. The balance of viscous and electrostatic forces provides a governing equation for small angular rotations of the dipole. The distant electric field so created can be predicted from the summed electrostatic potentials of the altered molecular dipoles.

The objective here is to quantitatively predict the magnitude of the resulting streaming potential and the corresponding EAG signal as a function of the fixed anion concentration in articular cartilage, the compression rate, and other fundamental physical and anatomical variables. The theoretical development has five parts: (1) analysis of stress and strain rate during cyclic loading of cartilage (2) accounting for viscous effects in fluid flow through cartilage (3) specifying a mechanism of radial displacement of sodium ions in atomic sodium-sulfonate dipoles (4) estimating the proportion of sodium ions susceptible to viscous nudging (5) integration of the resulting voltage signals from individual ion pairs in a cartilaginous disk. The goal of this approach is not to achieve high accuracy, but to obtain a working preliminary model that will provide insight into the molecular origin of macroscopic and measurable streaming potentials. Here classical physics (including Newton's law of viscosity and Coulomb's law of electrostatics) provides a good estimate of streaming potentials in cartilage, created by the balance of viscous and electrostatic forces acting at the molecular scale.

METHODS AND RESULTS

1. Cyclic loading of cartilage

The footprints of the femoral condyles on the medial and lateral tibial plateaus are roughly circular and located within the inner margins of the medial and lateral menisci[10], as sketched for a top view of the tibia in Figure 2(a). Here the loaded regions of articular cartilage are approximated as circular disks of radius, r_c , and uniform thickness h_c . Geometric variables are defined as shown in the Figures 2(b) and 2(c), and are described in the figure legend.

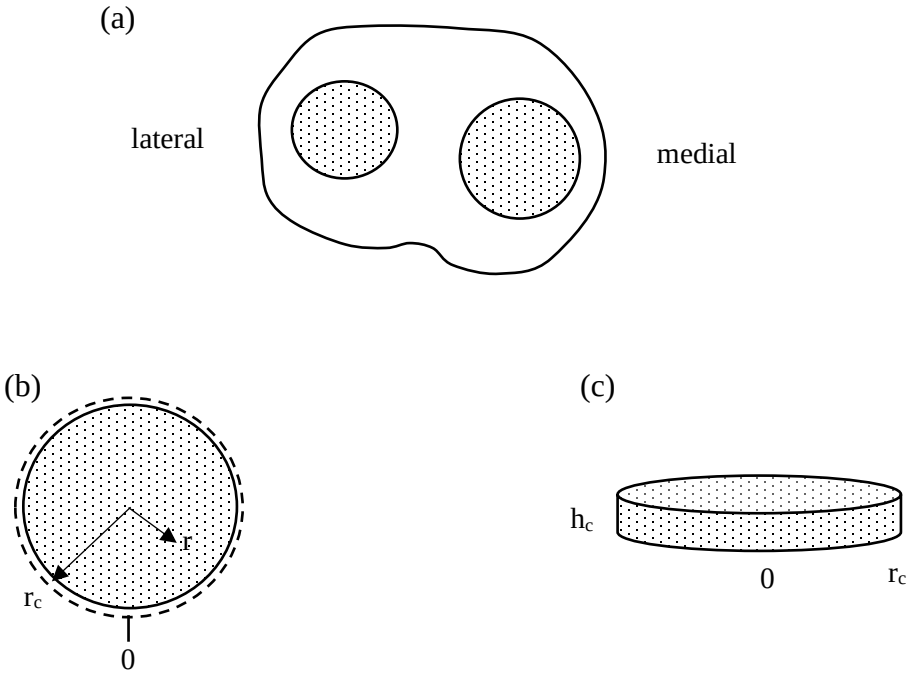

Figure 2. (a) Sketch a of top view of the contact area of a femoral condyle on the tibial plateau in a standing person. (b) Idealized circular contact area of articular cartilage under compressive load. Solid line indicates unloaded state. Dashed line shows compression and corresponding Poisson's ratio expansion under load (exaggerated for clarity). A variable distance between center and edge of the compressed zone is denoted r. (c) Perspective view showing coin-shaped disk of cartilage having unstressed vertical thickness h_c and radius r_c .

When a substantial fraction of body weight is rhythmically shifted to the contact area, the underlying articular cartilage is squeezed, undergoing compressive strain. Aqueous fluid moves radially away from center of the compression zone. Let

r = variable distance from center of disk
r_c = outer radius of the disk
h_c = uniform thickness of the disk
$\dot{\varepsilon}$ = compressive strain rate
α = volume fraction of water in cartilage.

Definitions and normal numerical values of these and other variables are summarized subsequently in Table 1. The qualitative mechanistic hypothesis of the present paper is that viscous force from trains of water molecules in a particular fluid lamina causes slight displacement of sodium ions in molecular dipoles that are formed by the sodium cations and their companion sulfonate anions. In aggregate, the resulting small displacements of the Na^+--R-SO_3^- molecular dipoles are the biophysical basis for the tiny electrical signals of the electroarthrogram. The fluid velocity and the velocity gradient in layers of water molecules passing through pores in the cartilage are therefore of particular importance.

Accordingly, the first objective is to derive an equation for the spatial mean outward velocity of water, $\bar{v}(r)$, at radial position, r , during cyclic loading as a function of compressive strain rate, $\dot{\varepsilon}$, in the cartilaginous disk of Figure 2. Consider the outward fluid flow at arbitrary radial distance, r , from the center of compression. The flow of water squeezed out radially is determined by the fluid volume swept out by compression perpendicular to the radius during time, dt . The spatial mean radial velocity is the rate of fluid volume displacement divided by the local macroscopic area perpendicular to flow,

$$\bar{v}(r) = \alpha \frac{\pi r^2 dh_c/dt}{2\pi r h_c} . \qquad (1)$$

Noting that strain rate

$$\dot{\varepsilon} = \frac{dh_c/dt}{h_c} , \qquad (2)$$

the radial fluid velocity at radius, r , is

$$\bar{v}(r) = \frac{1}{2}\alpha r \dot{\varepsilon} . \qquad (3)$$

During side-to-side weight shifting, the weight on the loaded cartilage steadily increases as more weight is shifted, so that $\dot{\varepsilon}$ remains approximately constant.

To determine the strain rate $\dot{\varepsilon} = \frac{dh_c/dt}{h_c}$, one can assume that the cyclic loading by side-to-side weight shifting causes quasi-static compression of the cartilage. That is, as the load gradually increases, the amount of strain increases according to Young's modulus of stiffness. The quasi-

static assumption is reasonable if compression is limited by the fibers of the cartilaginous matrix and not by resistance to outflow of water through pores in the matrix. The former condition is consistent with the work of Yan and coworkers[11] showing that Young's modulus increases nearly in direct proportion to dry/wet weight ratio, suggesting that it is the glycoprotein fiber content that provides stiffness[6].

For example, if a standing person rocks full body weight from side to side every 8 seconds, the loading and unloading times are 4 seconds each. Let

E_{dyn} = dynamic stiffness (Young's modulus or ratio of incremental stress to incremental strain at a particular load cycle frequency[7])
dP/dt = loading rate in terms of pressure per unit time
m = body mass
g = gravitational constant
T = half cycle time for loading or unloading
A_c = total contact area in one knee.

Then the compressive phase (or recoil phase) strain rate

$$\dot{\varepsilon} = \frac{d\varepsilon}{dt} = \frac{dP}{dt} \cdot \frac{d\varepsilon}{dP} = \frac{1}{E_{dyn}} \frac{dP}{dt} , \quad (4)$$

or

$$\dot{\varepsilon} = \frac{1}{E_{dyn}} \frac{dF}{dt} \cdot \frac{1}{A_c} \approx \pm \frac{1}{E_{dyn}} \frac{mg}{T/2} \cdot \frac{1}{A_c} . \quad (5)$$

As a numerical example, taking body mass as 70 kg in a typical adult patient, an average of measured values of E_{dyn} across publications of 18 MPa[12-15] (the individual studies reporting 3, 10, 10, and 50 MPa), half cycle time as 4 sec, and an estimate of total compression area for <u>both</u> medial and lateral compartments of the knee in one standing leg as 6.28 cm^2 ($2\pi \cdot 1\ cm^2$) we would have during acquisition of an electroarthrogram

$$\dot{\varepsilon} = \pm \frac{1}{18 \cdot 10^6 \frac{kg}{sec^2 \cdot m}} \frac{70\ kg \cdot 9.8 \frac{m}{sec^2}}{4\ sec} \cdot \frac{1}{0.000628\ m^2} = \pm 0.0152\ \frac{1}{sec} . \quad (6)$$

2. Viscous effects in flow through cartilage pores

The fluid viscosity describes the shear forces acting on parallel laminar sheets of fluid molecules. In the present model of cartilage, viscous effects slow local flow velocities near the walls of the small pores created between fibers in the cartilage matrix, as layers of water molecules rub against glycosaminoglycans lining the pores. Figure 3 illustrates a model pore as a short cylinder of radius $r_p \sim 50$ nm[16] in the cartilage matrix. Here the pore is an idealized model in which, under viscous conditions (Re <<1), a parabolic fluid velocity profile would develop having peak flow velocity at the center and near zero velocity flow at the wall. The idealized parabolic profile of the pore model is a mathematically tractable representation of the generally higher

flow velocities in the center of the pore than in "near-wall" fluid layers, where the molecular dipoles are located.

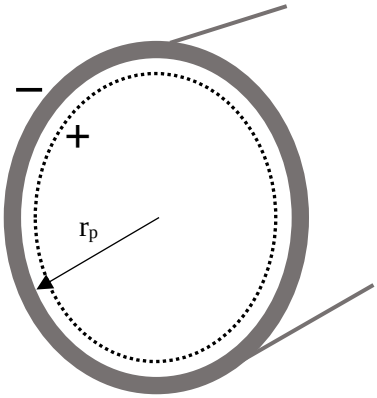

Figure 3. Sketch of an idealized fluid filled pore in the cartilage matrix used to account for fluid viscosity. Thick oval represents the pore wall containing fixed negative ions. Dotted oval represents a near-wall fluid lamina containing movable positive ions. r_p is the pore radius.

Consider laminar flow in a circular cross section through the pore, located at macroscopic radius, r , from the center of the disk of cartilage. As shown in Equation (3), the spatial mean flow velocity through the pore, $\bar{v}(r) = \frac{1}{2}\alpha r\dot{\varepsilon}$. We need to estimate the fluid velocity gradient near the edge of the pore, where the ionic dipoles are located. For the parabolic flow model, the velocity at the wall of the pore will be zero, and as is easily shown by calculus, the spatial mean flow velocity, $\bar{v}(r)$, over the pore area equals the local microscopic velocity through the pore at one half the pore radius. Let v' represent the local microscopic fluid velocity through the pore at arbitrary radius, r' , from the center of the pore. One can estimate the velocity gradient near the pore wall as

$$\frac{dv'}{dr'} \approx \frac{\Delta v'}{\Delta r'} = \frac{\bar{v}(r)}{r_p/2} = \frac{\frac{1}{2}\alpha r\dot{\varepsilon}}{r_p/2} = \alpha\frac{r}{r_p}\dot{\varepsilon} \,. \qquad (7)$$

For example, if $\alpha = 0.67$, $r_p = 50$ nm[16] , $r = 0.005$ m , and $\dot{\varepsilon} = 0.0152/\text{sec}$, then $dv/dr \approx 1018$ 1/sec. The parabolic flow assumption is an approximate way of representing the physical reality that laminar fluid flow in a viscous domain occurs slower near a fixed wall than in the central axis of flow. The next task is to focus on events in one particular lamina near the wall—the one containing the sodium ion of a sodium sulfonate molecular dipole.

3. Balance of forces nudging sodium ions in the direction of fluid flow

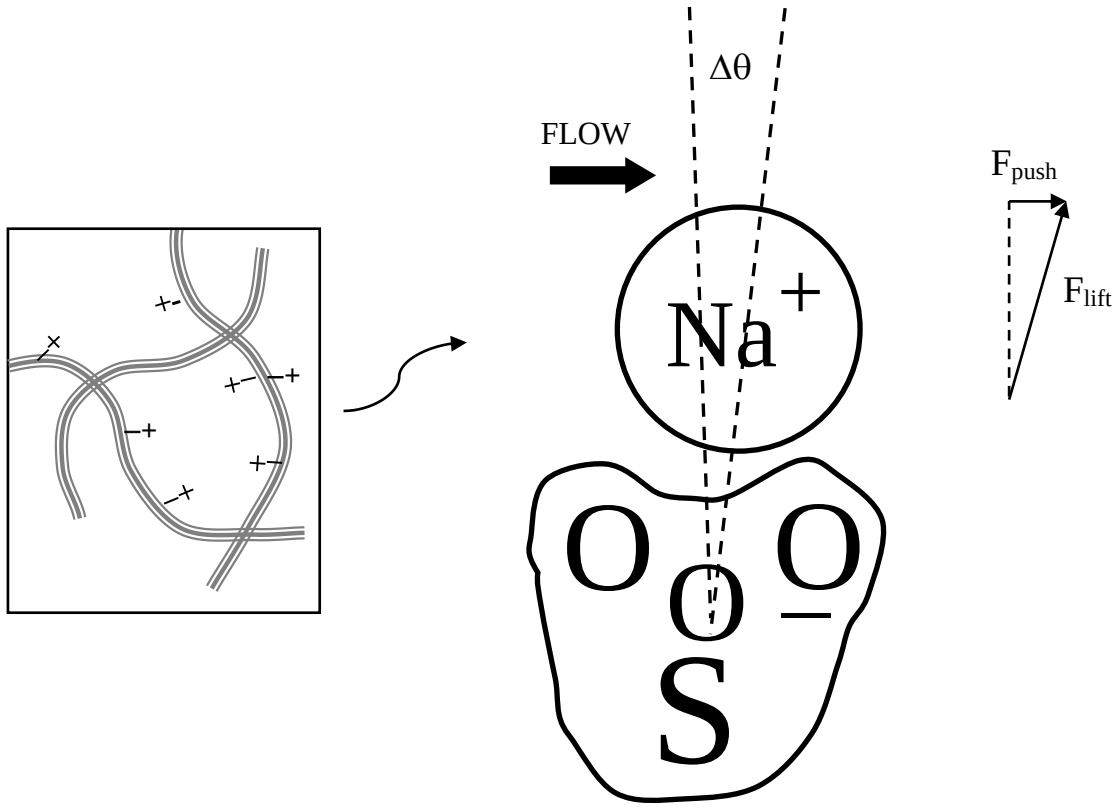

Figure 4. (Nanoscale, inset left) at the nanoscale fluid flows through openings in the cartilage matrix, perturbing mobile positive ions bound electrostatically to fixed anions. GAG decorations on collagen fibers create a fuzzy coating. (Atomic scale, right) an ion pair approximately perpendicular to flow within a particular viscous fluid lamina; a train of water molecules drags the positive sodium ion, nudging it and also lifting it slightly farther away from the negative sulfonate ion. Displacement angle, $\Delta\theta$, is greatly exaggerated for clarity.

Figure 4 (right) shows an atomic scale view of a sodium ion near the edge of a pore within a particular viscous lamina, as re-drawn from space filling molecular models. A small rub from the viscosity of fluid flow can cause slight displacement of the exposed positive ion. (As shown subsequently, such positive ions that are susceptible to nudging constitute about one half the total population of a random, three-dimensional distribution of dipoles.) The following section focuses on small viscous forces acting at the atomic scale.

The susceptible positive-negative ion pairs are approximately perpendicular to the direction of flow. The three oxygen atoms of the sulfonate ion form a shallow cup or socket, in which the sodium ion remains near a low energy equilibrium. Hence, the sodium ions do not flow freely with the moving fluid but rather sit in a potential energy well. To escape its low energy well the sodium ion would need to be lifted out of the socket formed by one sulfur and three oxygen atoms. The sulfonate ion has an approximately tetrahedral bond angle of 110 degrees, so the angle of the wall of the socket with respect to the fluid stream in a 90-degree perpendicular ion pair is in the range of 0 to (110 – 90), or 0 to 30 degrees. The mechanistic hypothesis of the present paper is that, at equilibrium (no further sodium ion motion) the forces of viscous pushing and electrostatic lifting balance so that $F_{lift} \sin \Delta\theta - F_{push} = 0$.

For the scheme of Figure 4 let

r_1 = the radius of the sulfonate ion
r_2 = the radius of the sodium ion
$d = r_1 + r_2$ = the distance between the two ions
Δd = the very small distance that the sodium ion is lifted uphill in the radial direction away from the sulfonate ion.

The electric field (Newtons/coulomb or Volts/m) of a point charge[17]

$$V = \frac{F}{q_1} = \frac{kQ_{source}q_1}{d^2} \cdot \frac{1}{q_1} = \frac{kQ_{source}}{d^2} = \frac{kq_1}{d^2}, \quad (8)$$

where in this problem $Q_{source} = q_1$ and

q_1 is one-unit charge (electron or proton) in Coulombs
F is the force acting on the unit charge
k is the permittivity constant[17], which is numerically equal to 9×10^9 Nt-m^2/Coul^2
Q_{source} is the central charge, which for this molecular dipole is equal to q_1 .

In the case of positive-negative ion pairs the force per unit charge is attractive, pulling the sodium ion closer to the sulfonate ion. Multiplying both sides of Equation (8) by q_1 , the force required to lift the sodium ion radially off of the sulfonate ion is

$$F_{lift} = \frac{kq_1^2}{d^2} \text{ Newtons} . \quad (8)$$

The water drags the positive ion downstream (Figure 4, right) until

$$F_{push} = F_{lift} \cdot \sin(\Delta\theta) \approx F_{lift}\Delta\theta \quad (9)$$

for very small average angular displacement, $\Delta\theta$, where $\sin(x) \approx x$ for $x << 1$. (Some dipoles will be moved more, some less, depending on their random starting angles.) In turn,

$$\Delta\theta = \frac{F_{push}}{\frac{kq_1^2}{d^2}} = \frac{F_{push}\, d^2}{kq_1^2}\,. \qquad (10)$$

This expression gives the rotation of the molecular dipole, as exposed sodium ions oriented perpendicular to water flow are nudged downstream. Other dipoles oriented parallel to water flow are shielded from viscous drag by neighboring atoms.

The next step is finding F_{push} in terms of the viscous force on the sodium ion in the direction of fluid flow. At no-flow equilibrium the sodium ion remains near a fixed position due to the balance of mechanical and electrical forces. Applying Newton's law of viscosity, $F_{push} \approx \mu(4\pi r_2^2)\frac{dv'}{dr'}$, where μ is the viscosity of water, $(4\pi r_2^2)$ is the surface area of a spherical sodium ion, r' is an arbitrary distance from the center of the pore, and v' is the local microscopic fluid velocity through the pore. Hence for near-wall velocity gradient, dv'/dr', of the local water layer

$$F_{push} \approx 4\mu\pi r_2^2 \frac{dv'}{dr'}\,, \qquad (11)$$

and using Equation (7) for $\frac{dv'}{dr'}$,

$$F_{push} \approx 4\alpha\mu\pi r_2^2 \frac{r}{r_p}\dot{\varepsilon} \qquad (12)$$

in correct units of Newtons, with r representing the macroscopic radial distance from the center of the disk. Now using Equation (12) in Equation (10), the slight rotation of the molecular dipole is

$$\Delta\theta(r) = \frac{F_{push}\, d^2}{kq_1^2} \approx \frac{4\alpha\mu\pi r_2^2 \frac{r}{r_p}\dot{\varepsilon}\cdot d^2}{kq_1^2}\,. \qquad (13)$$

There is a greater dipole angle shift at larger disk radii, r, associated with the faster fluid velocity at larger radii, r. Equation (13) describes the rotation of an ionic dipole that initially was oriented perpendicular to the direction of fluid motion. Sodium ions in dipoles oriented more parallel to fluid motion experience much less shear, because they are shielded by companion molecules.

4. Proportion of molecular dipoles susceptible to nudging

To estimate the fraction of molecular dipoles susceptible to nudging, consider the sketch of Figure 5, representing a random distribution of dipole orientations in three-dimensional space with respect to th direction of fluid flow.

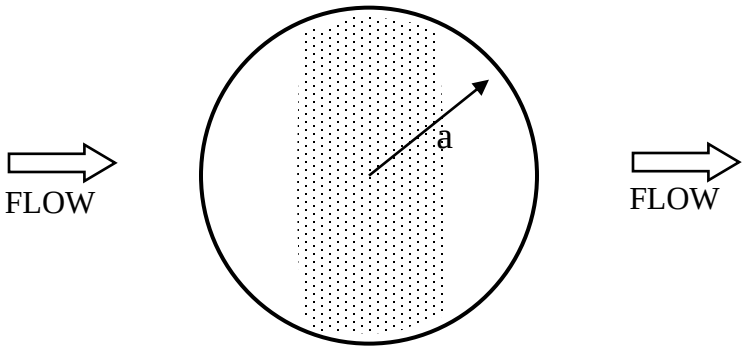

Figure 5. Sketch of a spherical distribution of vectors, having equal lengths, a , representing undisturbed dipole angles. Arrows indicate direction of potential flow.

In Figure 5 the shaded band represents those random dipoles approximately perpendicular to radial flow and susceptible to viscous drag. Of the entire spherical distribution of dipole angles in Figure 5, a proportion of them in a vertical band, perpendicular to flow within about one-half radius of the sphere center, will be subject to viscous shear and left-to-right displacement. Hence, the proportion of displaced molecular dipoles is approximately equal to the ratio of the surface area of the band to the surface area of the whole sphere,

$$\frac{2\pi a \cdot a}{4\pi a^2} \approx \frac{1}{2} . \qquad (14)$$

In this way we can estimate that for n molecular dipoles in a small microscopic volume of cartilage, about one half, or n/2 , will be susceptible to viscous nudging.

5. Effect of displaced dipoles on the far field electrical potential gradient

The next question is how will the slight changes in dipole angle from Equation (13) in any selected ion pair from the subpopulation in Equation (14) change the far field potential of the dipole, measured at electrode location, P , outside the disk of cartilage. Consider measured electrical potentials from a population of the dipoles in small sectors of cartilage oriented at different angles, as sketched in Figure 6. The dipoles perpendicular to radial fluid flow will be oriented at various angles from the center of the disk, ranging from 0 to 2π radians, as shown.

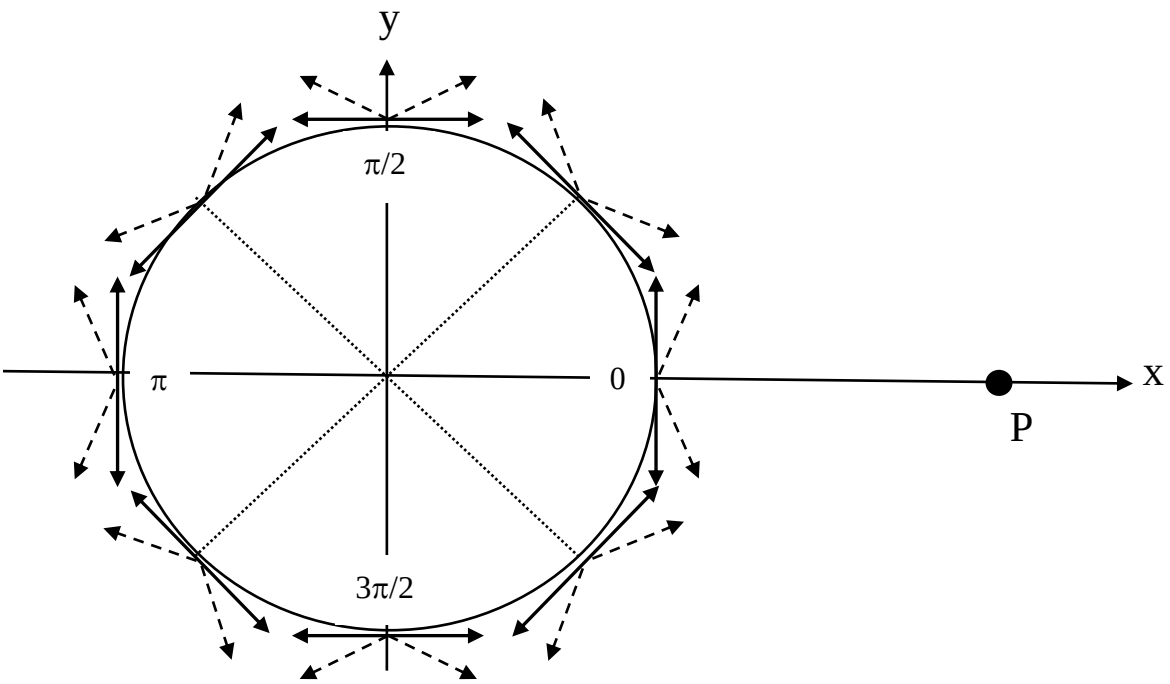

Figure 6. Orientation of flow mediated changes in molecular dipoles varies with their radial position. Molecular dipoles subject to drag forces are oriented in opposite directions, perpendicular to the local radius, owing to radial outflow of fluid. For dipoles on the x-axis at 0 and π radians the paired, mirror image dipoles are both shifted parallel to the x-axis, toward or away from measuring point, P . For dipoles on the y-axis at $\pi/2$ and $3\pi/2$ radians one mirror image dipole is shifted slightly toward P and the other is shifted slightly away from P , causing no net effect. For intermediate angles (dotted lines) the net effect is related to the cosine of the angle.

By deduction from Figure 6, in small tissue volumes at angle 0 all opposite-facing dipoles perpendicular to flow will be displaced toward P, creating a change from zero potential to a small positive potential. In similar small tissue volumes at angle π radians, all opposite-facing dipoles perpendicular to flow will be displaced away from P, creating a change from zero potential to a negative potential. In tissue volumes at angles $\pm \pi/2$ radians, half of the opposite-facing dipoles perpendicular to flow will be displaced toward P, and half will be displaced away from P equally, creating a net zero change in measured potential at P.

For simplicity, we can assume that most of the signal will be generated by the two sectors of the disk facing toward and away from P. This allows us to reduce a two-dimensional to a one-dimensional integration problem, by collapsing the dipoles in differential volumes of cartilage, $h_c\, r d\phi\, dr$, at distance r and angles $|\phi| < \pi/3$ radians or $\pm$ 60 degrees onto the x-axis (Figure 7). This trick will allow reasonable estimation of the aggregate potential at P from all of the dipoles in the differential volume. Consider molecular dipoles on the side of the disk closest to P that are shifted slightly toward P by fluid flow. The condensation of each finite element onto the x-axis creates an overestimate of the electrical potential at P by increasing the apparent contribution of dipoles at angles $|\phi| < 60$ degrees. These dipoles are assumed to be at minimal distance, $\lambda r_c - r$ from P, but they are actually at a slightly longer diagonal distance. However, ignoring positive contributions of dipoles at angles $|\phi| > 60$ degrees by assuming that they are equal to zero produces an underestimate of the electrical potential at P, creating offsetting errors that are reflected in the choice of $|\phi| < \pi/3$. Hence, this one-dimensional simplification is reasonable for a preliminary assessment of the viscous dipole nudging hypothesis.

The one-dimensional simplification of Figure 7 allows us to focus directly on the time-varying signal produced by shifting body weight from one knee to the other. The unstressed signal is near zero. Even if a non-zero background potential were present, it would not be time-varying. Any such constant, background voltage would be ignored or filtered out by voltage-sensing RC coupled preamplifiers like those used in recording the electrocardiogram.

Now consider an idealized geometric model of a cartilage disk shown in Figure 7 in more detail.

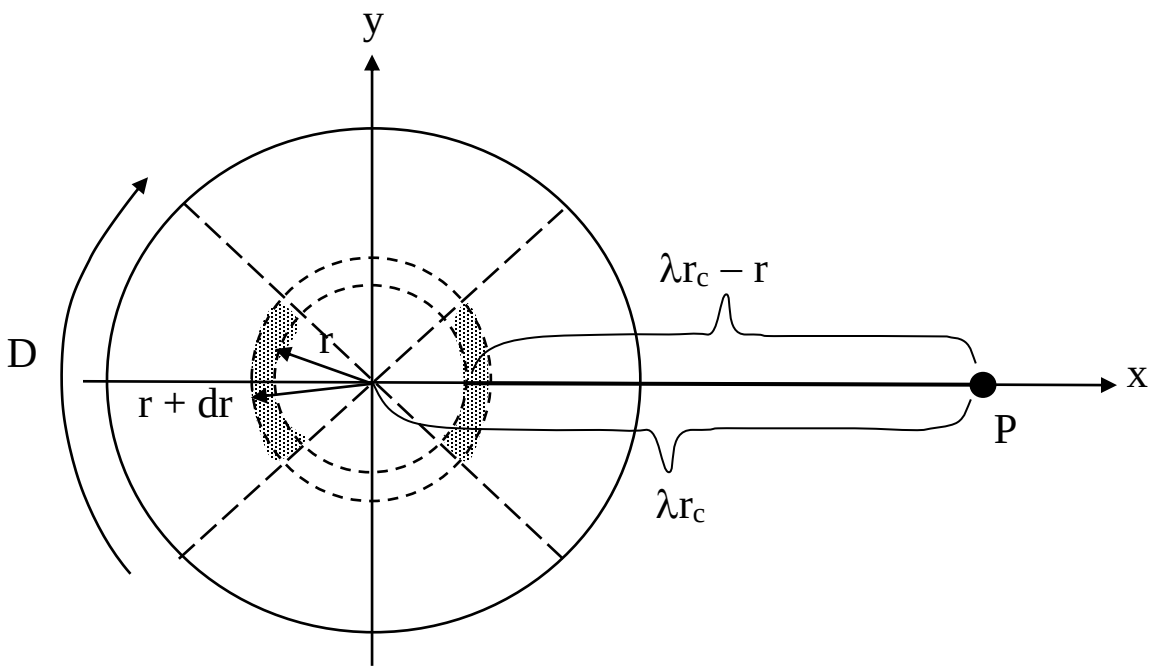

Figure 7: Top view of cartilage disk of thickness, h_c , with scheme for calculating the summed streaming dipole potential at electrode location, P , located λ disk radii away. Angle D represents a sector of the disk that is generating most of the voltage signal at P from displaced molecular dipoles. The outer radius of the disk is r_c . λr_c represents the distance between the center of the disk and P. An arbitrary inner radial position is denoted r . $\lambda r_c - r$ represents the straight line distance between the shaded differential volume element, $h_c\, r d\phi\, dr$, and point P. The height of the disk (not shown) is denoted h_c .

We wish to find the signal at the electrode location denoted P from an average molecular dipole in the differential volume of the disk, $h_c\, r d\phi\, dr$, subject to the slight changes in dipole angle from Equation (13). Here the term "electrode" means the positive input electrode at point, P, near the joint, rather than the more distant reference electrode on the leg.

In Figure 7 the shaded volumes represent the differential sectors of the disk facing toward or away from P that generate the large majority of voltage changes at point P. The right hand volume at a particular positive value of x generates a positive signal at P, and being farther away, the left hand volume at the corresponding negative value of x generates a smaller negative signal at P.

As is well-known[17], the far field electric potential at distance, λr_c , would be

$$V_1 = \frac{kq_1 d}{(\lambda r_c - r)^2} \cos\psi \,, \tag{15}$$

where, for a single charge molecular dipole, q_1 represents one positive charge in units of Coulombs, d represents the distance between the positive and negative charges of the dipole, and angle ψ represents the angle between the dipole axis and P. The cosine function means that dipoles directly facing toward P with angle 0 radians create maximal positive potential. Dipoles facing directly away from P with angle π radians have maximal negative potential. Dipoles pointing at right angles to P with angles $\pm \pi/2$ create zero potential.

Displaced dipoles facing toward the sensing electrode each create a positive change in electrostatic potential gradient, V_1, at the electrode. Displaced dipoles facing away from the sensing electrode each create a negative change in potential gradient, V_1, at the electrode. As shown in Figure 6, the signal at P is generated in sectors of the cartilage disk facing toward or away from the electrode in proportion to the function $\cos\psi$.

Now imagine the change in EAG potential recorded at point, P , from a single molecular dipole. Let the dipole be oriented at any arbitrary angle, ψ , in three-dimensional space with respect to the x-axis. During cyclic loading,

$$\Delta V_1(\psi - \Delta\theta(r)) = \frac{kq_1 d}{(\lambda r_c - r)^2} \cos(\psi - \Delta\theta(r)) \text{ , or}$$

$$\Delta V_1(r) = \frac{kq_1 d}{(\lambda r_c - r)^2} [\cos(\psi)\cos(\Delta\theta(r)) + \sin(\psi)\sin(\Delta\theta(r))] \,, \tag{16}$$

which, with small angle approximations for the sine and cosine, gives

$$\Delta V_1(r) = \frac{kq_1 d}{(\lambda r_c - r)^2} [\cos(\psi) \cdot 0 + \sin(\psi) \cdot \Delta\theta(r)] \ . \tag{17}$$

The voltage signal during the compression phase is therefore

$$\Delta V_1(r) \approx \frac{kq_1 d}{(\lambda r_c - r)^2} \sin(\psi) \cdot \Delta\theta(r) \ . \qquad (18)$$

For dipoles roughly perpendicular to "east-west" flow along the x-axis toward or away from P, $\psi \approx \frac{\pi}{2}$, and $\sin(\psi) \approx 1$. This approximation is valid because viscous drag is minimal for dipole angles substantially different from ± 90 degrees or ± π/2 radians with respect to the direction of flow. So, we have

$$\Delta V_1(r) \approx \frac{kq_1 d}{(\lambda r_c - r)^2} \Delta\theta(r) \ . \qquad (19)$$

This is the shift in far field potential caused by the small change in dipole orientation with fluid streaming. Here $\Delta\theta$ is considered a step function in time produce by cyclic loading. $\Delta\theta$ is positive during loading and negative during unloading, that is, positive during compression and negative during decompression.

Now we can substitute for $\Delta\theta$ using Equation (13), namely

$\Delta\theta(r) = \frac{4\alpha\mu\pi r_2^2 \frac{r}{r_p} \dot{\varepsilon} \cdot d^2}{kq_1^2}$, so that during loading or unloading ($\dot{\varepsilon} > 0$ or $\dot{\varepsilon} < 0$)

$$\Delta V_1(r) = \frac{kq_1 d}{(\lambda r_c - r)^2} \cdot \frac{4\alpha\mu\pi r_2^2 \frac{r}{r_p} \dot{\varepsilon} \cdot d^2}{kq_1^2} \ , \text{ or} \qquad (20)$$

$$\Delta V_1(r) = \frac{r}{(\lambda r_c - r)^2} \cdot \frac{4\alpha\mu\pi r_2^2 \dot{\varepsilon} \cdot d^3}{r_p q_1} \ . \qquad (21)$$

The number of individual dipoles in the differential volume element of Figure 7 with dimensions h_c rD dr = h_c |x|D dx is dn = ch_c D|x| dx , where c denotes the concentration of sodium sulfonate ions forming ionic dipoles. Angle D, defined in Figure 7, specifies the full range of sectors facing toward or away from P that produce significant EAG signals. Here arbitrary radius, r , is equal to |x| in the condensed one-dimensional model of Figure 7. The symbol |x| works for both positive and negative values of x in Figure 7 to give values of dn > 0. If dn/2 of the dipoles are susceptible to nudging, then the differential volume of movable molecular dipoles will produce the aggregate signal $dV(x) = \Delta V_1(x) \frac{dn}{2}$, namely

$$dV(x) \approx \frac{x}{(\lambda r_c - x)^2} \cdot \frac{4\alpha\mu\pi r_2^2 \dot{\varepsilon} \cdot d^3}{r_p q_1} \cdot \frac{cDh_c|x|dx}{2}, \text{ or} \qquad (22)$$

$$dV(x) \approx \frac{4\alpha\mu\pi r_2^2 \dot{\varepsilon} \cdot d^3 cDh_c}{2r_p q_1} \cdot \frac{x|x|}{(\lambda r_c - x)^2} \, dx \equiv Kh_c \frac{x|x|}{(\lambda r_c - x)^2} dx \ . \qquad (23)$$

In Equation (23) the lumped constant, $K = \frac{2\alpha\mu\pi r_2^2 \dot{\varepsilon} \cdot d^3 cD}{r_p q_1}$, represents the physical and electrical properties of the cartilage. Equation (23) gives the incremental change in voltage, dV , caused by fluid flow during loading or unloading of a condensed dx-thick slice at distance x. The total change in observed electrical potential, V, across the disk can be easily computed by numerical integration of this expression.

From Equation (23) we have $dV(x) \approx Kh_c \frac{x|x|}{(\lambda r_c - x)^2} dx$ including the absolute value term, which comes from the positive number of dipoles in a condensed, dx-thick slice. For cases of $x \geq 0$ the contribution is positive. For cases of $x < 0$ the contribution is negative. To deal with the negative values of x in the numerator and the denominator, the aggregate voltage signal from all slices of the disk is

$$V = \int_{-r_c}^{r_c} dV(x) \approx Kh_c \int_{-r_c}^{r_c} \frac{x|x|}{(\lambda r_c - x)^2} dx = Kh_c \left[\int_0^{r_c} \frac{x^2\, dx}{(\lambda r_c - x)^2} - \int_0^{r_c} \frac{x^2\, dx}{(\lambda r_c + x)^2} \right]. \quad (24)$$

Here the expression,

$$V = Kh_c \left[\int_0^{r_c} \frac{x^2\, dx}{(\lambda r_c - x)^2} - \int_0^{r_c} \frac{x^2\, dx}{(\lambda r_c + x)^2} \right] \quad (25)$$

accounts for the absolute value |x| in Equation (24). As shown in the APPENDIX, applying the polynomial approximation in[18], namely,

$$\frac{1}{(1 \pm \epsilon)^2} \approx 1 \mp 2\epsilon + 3\epsilon^2 , \ \epsilon^2 < 1 , \quad (26)$$

$$V \approx K \frac{h_c r_c}{\lambda^3} . \quad (27)$$

If $r_c = 0$ or $h_c = 0$, then there is no disk, and V = 0. If r_c and r_c are finite and $\lambda \to \infty$, then V = 0 in this limiting case as well. The constant, K , describes effects of physical and electrical properties of the cartilage and the compressive strain rate. Constants, r_c, h_c , and λ describe the geometric properties of the knee and the sensing electrode.

Note that for a complete rocking cycle of the EAG, there are both positive and negative phases of strain during loading and unloading. The signal is positive during loading and negative during unloading. This means that the peak-to-peak EAG signal amplitude, as seen on graphic recordings, would be 2V or

$$V_{pp} \approx 2K \frac{r_c h_c}{\lambda^3} . \quad (28)$$

6. Numerical methods

Two specific test cases were modeled: a normal human subject and a patient with moderate to severe osteoarthritis with uniform thinning of the cartilage. All model parameters were determined from known physical constants and known anatomy. There are no free parameters. There are no arbitrary constants.

Numerical values of the model parameters for the normal knee are shown in Table 1. For the case of uniform osteoarthritis, the thickness was reduced by 80% from 6 mm to 1.2 mm. Fixed anion concentration and Young's modulus were both reduced to 0% of normal, as described by Nia and colleagues[19] with offsetting effects on constant, K .

Table 1: Standard Normal Model Parameters

Symbol	Property (kms units)	Numerical value
α	Proportion of water in disk	0.67
c	Concentration of fixed anions in cartilage (mol/m^3)	218 **
c	Concentration of fixed anions in cartilage ($atoms/m^3$)	1.3E+26
d	Distance between ions in dipole (m)	0.5E-9
D	Angle for one dimensional approximation (radians)	2.09
E_{dyn}	Dynamic stiffness of cartilage tissue (Pascals)	18E+6 *
$\dot{\varepsilon}$	Compressive strain rate (1/sec)	0.0152
h_c	Normal disk height (m)	0.006
g	Gravitational constant (m/sec^2)	9.8
k	Electrostatic constant ($Nt\text{-}m^2/Cloul^2$)	9.0E+9
λr_c	Distance from disk center to measuring point, P (m)	0.020
N_A	Avogadro's number	6E+23
m	Body mass of typical adult human (kg)	70
μ	Viscosity of water at 37 deg C ($N\text{-}sec/m^2$)	0.00068
q_1	One ionic charge (Coulombs)	1.6E-19
r_2	Radius of positive sodium ion (m)	0.25E-9
r_c	Disk radius (m)	0.01
r_p	Radius of fluid filled pore in cartilage (m)	50E-9

* Average dynamic stiffness from references[12-15] representing stress-strain curves over the range of normal body weight.

** Venn[20] found a fixed charge density of healthy cartilage of about 125 mEq/kg wet weight or 0.125 molar. Kiviranta[21] found an average value of 250 mEq/L of fixed negative charge in elaborate histochemical studies. Lesperance[22] measured a fixed charge density in cartilage of 280 mEq/L. An average value for fixed negative charges healthy, normal cartilage would be 218 mM, which is also consistent with the data of Lu[23].

7. Preliminary results

The average tilt or change in dipole angle at the edge of the cartilage disk toward the direction of flow, calculated from Equation (16), at radius r = 1 cm on the edge of the disk was $\Delta\theta = \frac{4\alpha\mu\pi r_2^2 \frac{r_c}{r_p}\dot{\varepsilon}\cdot d^2}{kq_1^2} = \ 1.2 \cdot 10^{-9}$ radians. Nevertheless, this small change was sufficient to produce macroscopically measurable streaming potentials.

Figure 8 shows the relative contributions to the overall measured potential, V, of dx-thick regions along the x-axis. Areas on the near side of the disk, closer to the electrode at P , cause larger positive changes in measured potential. Areas on the far side of the disk, farther from the electrode at P , cause smaller negative changes in measured potential.

Table 2 shows simulated peak-to-peak EAG on the skin surface at the medial joint line for normal and abnormal test cases. The computed values in Table 2 correspond to experimentally measured EAG signals on the skin surface at the medial joint line reported by Preville and coworkers[1]. The simulated peak-to-peak EAG in a normal patient model was 0.174 mV. Experimental peak-to-peak EAG amplitude for normal control patients was 0.231 ± 0.077 mV. The simulated peak-to-peak EAG in patients with moderate to severe osteoarthritis was 0.035 mV. Experimental peak-to-peak EAG for patients with advanced osteoarthritis prior to joint replacement was 0.057 ± 0.043 mV. The agreement of preliminary calculations with human data supports the proposed mechanism of streaming potentials in cartilage.

Table 2: Simulated EAG potentials at the medial joint line

Test case	EAG signal (mV)
Normal knee	0.174
Moderate to severe osteoarthritis	0.035

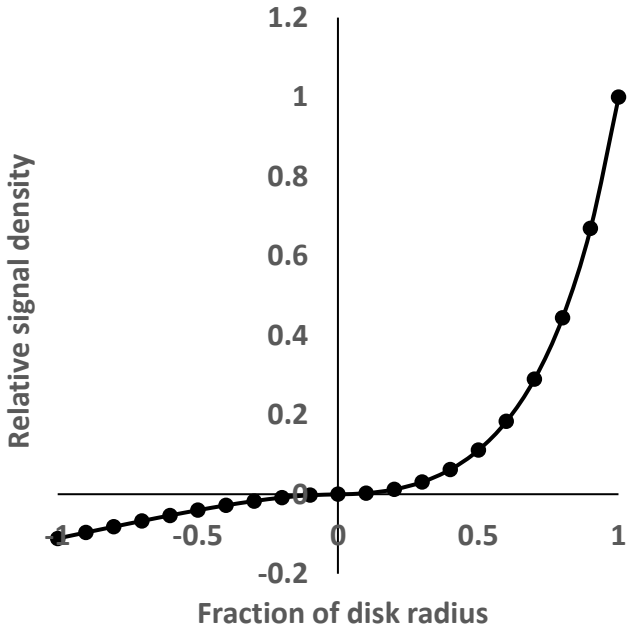

Figure 8. Relative contributions of dx-thick slices of cartilage perpendicular to the x-axis to the overall normal EAG signal, measured at point P in Figure 7.

DISCUSSION

The forgoing analysis provides a new quantitative model of streaming potentials in the electroarthrogram, based upon first-principles of physics. The model predicts that the streaming potential from the center of the compression zone to the outer edge is proportional to the loading rate, represented by mg/T, fixed anion concentration, c , the radius of the cartilage disk, r_c , and the thickness of the cartilage disk, h_c . The measured streaming potential is inversely related to the cartilage stiffness (E_{dyn}) and the cube of the relative electrode distance, λ , from the center of the cartilage.

Assuming temporarily that the underlying molecular and biophysical mechanisms are sound, the algebraic forms of Equations (3), (4), and (28) reveal interesting aspects of the EAG system. Based upon Equation (28) and the shapes of the curves in Figure 8, the EAG appears to be an indirect linear measure of the diameter and thickness of the cartilage. Further, the signal is generated mostly by tissue near the outer rim that is facing the electrode on the skin surface.

In late-stage osteoarthritis a key abnormality in osteoarthritis is loss of sulfonate groups in articular cartilage[2]. Glycosaminoglycans become severely depleted, and fixed anion concentration, c , decreases. In the present model the EAG is proportional to c . However, the EAG is also proportional to the strain rate, $\dot{\varepsilon} = \frac{1}{E_{dyn}} \frac{mg}{T/2} \cdot \frac{1}{A_c}$, which is an inverse function of cartilage stiffness, E_{dyn} . Both stiffness and fixed anion concentration are known to decrease in

osteoarthritis[2]. These changes, reflected by the ratio c/E_{dyn} , should have offsetting effects upon voltage amplitudes of the EAG, with lumped constant, K, roughly unchanged. Thus, the EAG may not be especially sensitive in detecting early, asymptomatic osteoarthritis. However, the EAG, which is expected be proportional to local thickness, h_c , may be able to detect or to inexpensively monitor more severe disease with joint space narrowing. EAG measurements are very sensitive to electrode placement. Doubling the sensing electrode distance in terms of disk radii, λ , reduces the EAG signal by a factor of eight. Despite the complexity of the underlying biophysics and the many contributing factors in Table 1 and in Equation (28), the present relatively simple electro-mechanical model may be useful in understanding and interpreting the significance of electroarthrograms.

CONCLUSIONS

Compression and fluid flow in cartilage can generate predictable electric fields. The preliminary electro-kinetic model, summarized in Equation (28), provides a simple algebraic expression for of the physical variables that determine streaming potentials between the center and the periphery of compressed knee joint cartilage. The model has no adjustable parameters or arbitrary constants and provides a first-principles solution to the forward problem of electroarthrography—predicting the electrical signal recorded at a distance, given detailed specification of the source. Knowledge of the relevant parameters that govern the streaming potentials produced by cyclic compression and relaxation of articular cartilage may inform the use of electroarthrography as a noninvasive diagnostic test.

REFERENCES

1. Preville AM, Lavigne P, Buschmann MD, Hardin J, Han Q, Djerroud L, Savard P (2013). Electroarthrography: A novel method to assess articular cartilage and diagnose osteoarthritis by non-invasive measurement of load-induced electrical potentials at the surface of the knee. Osteoarthritis Cartilage 21, 1731-1737.
2. Hileman RE, Fromm JR, Weiler JM, Linhardt RJ (1998). Glycosaminoglycan-protein interactions: Definition of consensus sites in glycosaminoglycan binding proteins. Bioessays 20, 156-167.
3. Hardingham TE, Fosang AJ, Dudhia J (1990). Domain structure in aggregating proteoglycans from cartilage. Biochem Soc Trans 18, 794-796.
4. McDevitt CA (1973). Biochemistry of articular cartilage. Nature of proteoglycans and collagen of articular cartilage and their role in ageing and in osteoarthrosis. Ann Rheum Dis 32, 364-378.
5. Grodzinsky AJ, Lipshitz H, Glimcher MJ (1978). Electromechanical properties of articular cartilage during compression and stress relaxation. Nature 275, 448-450.
6. Palmer AW, Guldberg RE, Levenston ME (2006). Analysis of cartilage matrix fixed charge density and three-dimensional morphology via contrast-enhanced microcomputed tomography. Proc Natl Acad Sci U S A 103, 19255-19260.
7. Ahsanizadeh S, Li L (2015). Strain-rate-dependent non-linear tensile properties of the superficial zone of articular cartilage. Connect Tissue Res 56, 469-476.
8. Frank EH, Grodzinsky AJ, Koob TJ, Eyre DR (1987). Streaming potentials: A sensitive index of enzymatic degradation in articular cartilage. J Orthop Res 5, 497-508.

9. Frank EH, Grodzinsky AJ (1987). Cartilage electromechanics--ii. A continuum model of cartilage electrokinetics and correlation with experiments. J Biomech 20, 629-639.
10. Scarvell JM, Smith PN, Refshauge KM, Galloway HR, Woods KR (2004). Comparison of kinematic analysis by mapping tibiofemoral contact with movement of the femoral condylar centres in healthy and anterior cruciate ligament injured knees. J Orthop Res 22, 955-962.
11. Yan D, Zhou G, Zhou X, Liu W, Zhang WJ, Luo X, Zhang L, Jiang T, Cui L, Cao Y (2009). The impact of low levels of collagen ix and pyridinoline on the mechanical properties of in vitro engineered cartilage. Biomaterials 30, 814-821.
12. Burgin LV, Edelsten L, Aspden RM (2014). The mechanical and material properties of elderly human articular cartilage subject to impact and slow loading. Med Eng Phys 36, 226-232.
13. Mansfield JC, Bell JS, Winlove CP (2015). The micromechanics of the superficial zone of articular cartilage. Osteoarthritis Cartilage 23, 1806-1816.
14. Park S, Hung CT, Ateshian GA (2004). Mechanical response of bovine articular cartilage under dynamic unconfined compression loading at physiological stress levels. Osteoarthritis Cartilage 12, 65-73.
15. Vazquez KJ, Andreae JT, Henak CR (2019). Cartilage-on-cartilage cyclic loading induces mechanical and structural damage. J Mech Behav Biomed Mater 98, 262-267.
16. DiDomenico CD, Lintz M, Bonassar LJ (2018). Molecular transport in articular cartilage - what have we learned from the past 50 years? Nat Rev Rheumatol 14, 393-403.
17. Kip AF (1969). Fundamentals of electricity and magnetism. McGraw-Hill: New York.
18. Selby SM (1975). CRC standard mathematical tables. Cleveland.
19. Nia HT, Bozchalooi IS, Li Y, Han L, Hung HH, Frank E, Youcef-Toumi K, Ortiz C, Grodzinsky A (2013). High-bandwidth afm-based rheology reveals that cartilage is most sensitive to high loading rates at early stages of impairment. Biophys J 104, 1529-1537.
20. Venn M, Maroudas A (1977). Chemical composition and swelling of normal and osteoarthrotic femoral head cartilage. I. Chemical composition. Ann Rheum Dis 36, 121-129.
21. Kiviranta I, Jurvelin J, Tammi M, Saamanen AM, Helminen HJ (1985). Microspectrophotometric quantitation of glycosaminoglycans in articular cartilage sections stained with safranin o. Histochemistry 82, 249-255.
22. Lesperance LM, Gray ML, Burstein D (1992). Determination of fixed charge density in cartilage using nuclear magnetic resonance. J Orthop Res 10, 1-13.
23. Lu XL, Sun DD, Guo XE, Chen FH, Lai WM, Mow VC (2004). Indentation determined mechanoelectrochemical properties and fixed charge density of articular cartilage. Ann Biomed Eng 32, 370-379.

APPENDIX -- Integration of EAG signal components with absolute value of x

From Equations (24) and (25) we have $V = Kh_c\left[\int_0^{r_c} \frac{x^2\,dx}{(\lambda r_c - x)^2} - \int_0^{r_c} \frac{x^2\,dx}{(\lambda r_c + x)^2}\right]$, which can be put in the form

$$V = Kh_c \int_0^{r_c} \frac{x^2}{\lambda^2 r_c^2}\left(\frac{1}{\left(1-\frac{x}{\lambda r_c}\right)^2} - \frac{1}{\left(1+\frac{x}{\lambda r_c}\right)^2}\right) dx\,. \qquad (29)$$

Equation (29) can be greatly simplified and made more user friendly by applying a 2-term polynomial approximation, based on the series expansion $\frac{1}{(1\pm\epsilon)^2} \approx 1 \mp 2\epsilon + 3\epsilon^2$, $\epsilon^2 < 1$. In Equation (29) x is always less than λr_c, because the sensing electrode on the skin surface is always located outside the radius of the cartilage disk. So,

$$V \approx Kh_c \int_0^{r_c} \frac{x^2}{\lambda^2 r_c^2}\left(1 + 2\frac{x}{\lambda r_c} + 3\left(\frac{x}{\lambda r_c}\right)^2 - \left(1 - 2\frac{x}{\lambda r_c} + 3\left(\frac{x}{\lambda r_c}\right)^2\right)\right) dx\ , \qquad (30)$$

or

$$V \approx Kh_c \int_0^{r_c} \frac{x^2}{\lambda^2 r_c^2}\left(4\frac{x}{\lambda r_c}\right) dx = Kh_c \frac{4}{\lambda^3 r_c^3}\int_0^{r_c} x^3 dx\ , \qquad (31)$$

so that the simulated EAG half-signal during the positive phase of joint compression

$$V \approx \frac{Kh_c r_c}{\lambda^3}\ . \qquad (32)$$